Journal of Hazardous Materials 373 (2019) 141–151

Contents lists available at ScienceDirect

Journal of Hazardous Materials

journal homepage: www.elsevier.com/locate/jhazmat

An efficient mechanochemical synthesis of alpha-aluminum hydride: Synergistic effect of TiF_3 on the crystallization rate and selective formation of alpha-aluminum hydride polymorph

Congwen Duan[a,b,*], Yizheng Cao[c], Lianxi Hu[d], Dong Fu[a,b,*], Jinlong Ma[e], Jeffrey Youngblood[f]

[a] Hebei Key Lab of Power Plant Flue Gas Multi-Pollutants Control, Department of Environmental Science and Engineering, North China Electric Power University, Baoding, 071003, PR China
[b] MOE Key Laboratory of Resources and Environmental Systems Optimization, College of Environmental Science and Engineering, North China Electric Power University, Beijing, 102206, PR China
[c] SSCI, Albany Molecular Research Inc., West Lafayette, IN 47906, USA
[d] School of Materials Science and Engineering, Harbin Institute of Technology, Harbin, 150001, China
[e] School of Information Science and Engineering, Hebei University of Science and Technology, Shijiazhuang, 050018, China
[f] School of Materials Engineering, Purdue University, West Lafayette, IN 47907, USA

GRAPHICAL ABSTRACT

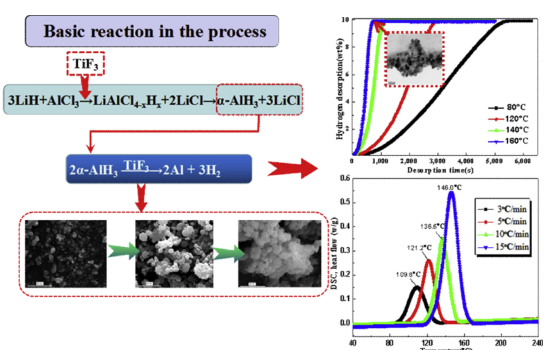

ARTICLE INFO

Keywords:
Synergistic effect
Mechanochemical reaction
α-AlH_3 nano-composite
Dehydriding property

ABSTRACT

α-AlH_3 is one of the most promising hydrogen storage materials due to its high gravimetric hydrogen capacity and low dehydriding temperature. In present work, a convenient and cost-efficient solid-state mechanochemical reaction is proposed to obtain α-AlH_3 nano-composite. With the addition of TiF_3, α-AlH_3 nano-composite was formed in a short period by milling of LiH and $AlCl_3$. Based on XRD and NMR results, the average grain size of the α-AlH_3 in the nano-composite was 45 nm. The reaction pathway as well as the synergistic effect of TiF_3 on the solid state reaction between LiH and $AlCl_3$ were confirmed. In the α-AlH_3/LiCl nano-composite, TiF_3 reduced the temperature of dehydriding reaction and improved dehydrogenation rate of α-AlH_3. Within the temperature range between 80 and 160 °C, dehydrogenation of the as-milled α-AlH_3 nano-composite showed fast kinetics. At 160 °C, a maximum hydrogen desorption of 9.92 wt% was obtained within 750 s, very close to the theoretical hydrogen capacity of α-AlH_3.

* Corresponding authors at: Hebei Key Lab of Power Plant Flue Gas Multi-Pollutants Control, Department of Environmental Science and Engineering, North China Electric Power University, Baoding, 071003, PR China.
E-mail addresses: duancw@ncepu.edu.cn (C. Duan), fudong@ncepu.edu.cn (D. Fu).

https://doi.org/10.1016/j.jhazmat.2019.03.064
Received 29 November 2018; Received in revised form 11 February 2019; Accepted 14 March 2019
Available online 15 March 2019

1. Introduction

Hydrogen, as a clean and renewable energy source, has received wide attention [1–3]. However, the major obstacle for a widespread hydrogen utilization is the challenges in storage [4]. The hydrogen storage technology includes gas storage, liquid storage and solid-state hydrogen storage method which is different from other storage technologies such as CO_2 adsorption and storage technology [1,5,6]. Solid-state hydrogen storage methods offer advantages, such as the lower safety risk, over high-pressure and cryogenic approaches [7]. Additionally, solid materials have excellent volumetric and gravitational storage capacities. Therefore, a lot of efforts have been undertaken in research and development of solid-state hydrogen storage materials as well as storage systems [8–16]. Research of safe, recyclable and cheap hydrogen storage materials, such as the light metal hydrides and their complexes, is the focus of the most recent studies; however, several issues still remain unsolved [4,10–12]. Aluminum trihydride (AlH_3), also known as alane, has a large hydrogen capacity (about 10 wt%) as well as a high volumetric density equal to 148 kg/m^3 of hydrogen [17–21], both of which exceed United States Department of Energy (US DOE) requirements, i.e., 7.5 wt.% and 70 g/l [7,20,22,23]. AlH_3 completely decomposes with a desirable rate at relatively low temperatures (100–200 °C), which is essential for the compatibility requirements with proton-exchange membrane fuel cells [24]. AlH_3 releases hydrogen leaving only metallic Al, a residue that is convenient to recycle. Thus, similar to RhAu, carbon nanotubes and transition metal composites [25–32], AlH_3 is considered as an excellent reversible hydrogen storage source with potential applications in rocket and fuel cell industries [33–37].

Currently, seven different polymorphs for AlH_3 are known: α, α', β, γ, δ, ε and ζ [38–46]. All but α-polymorph are metastable at ambient conditions. α-AlH_3 is the most studied polymorph because of the high stability. It is stable at room temperature but thermodynamically unstable at 150 °C under 10 kbar [40]. Although AlH_3 has many promising attributes, it is still not fully utilized as a hydrogen storage material, mainly because of the lack of an efficient and convenient industrial production method. Until 1976, the most popular methods to prepare AlH_3 polymorphs were the wet chemical synthesis proposed by Brower et al. It involved $LiAlH_4$ and $AlCl_3$ as the starting materials and $LiBH_4$ as a desolvation aid, and ether as the solvent. Alane- ether complexes form according to Eq. (1) [47]:

$$3LiAlH_4 + AlCl_3 + nEt_2O \rightarrow 4AlH_3{\cdot}nEt_2O + 3LiCl \quad (1)$$

Bulychev et al. [48–50] later modified this method and synthesized AlH_3 by reacting lithium aluminum hydride ($LiAlH_4$) with a strong acid like sulfuric acid (H_2SO_4) in ether, with crystallization from diethyl ether-benzene solution (see Eq. (2)):

$$2LiAlH_4 + H_2SO_4 \rightarrow 2AlH_3 + Li_2SO_4 + 2H_2 \quad (2)$$

In general, AlH_3 can be synthesized from alkali and/or alkaline earth metal tetrahydroaluminates, or hydrides based on wet chemical reactions [45–47] through the formation of alane–ether complexes. However, despite being less expensive and/or very reactive, these methods of α-AlH_3 synthesis involve large amounts of environmentally harmful organic solvents, and are highly sensitive to temperature and time. It is impractical to handle volatile organic liquids and the methods are not suitable for large-scale AlH_3 production. Thus, a solvent-free synthesis yielding non-solvated and adduct-free AlH_3 is highly desirable.

Saitoh reported synthesis of adduct-free AlH_3 by hydrogenation of Al (see Eq. (3)) [51]. However, this method can only be accomplished under H_2 pressure with at least 10 GPa at 25 °C because of the stabilizing surface aluminum oxide layer or low diffusivity of hydrogen [34]. Saitoh also demonstrated a H_2 pressure as high as 6 GPa at 300–800 °C could be used to perform efficient Al hydrogenation [52]. Thermodynamically, hydrogenation of Al to obtain AlH_3 is not a preferred method. Thus, such high pressures during AlH_3 synthesis make this method less attractive for large-scale AlH_3 synthesis.

$$2Al + 3H_2 \rightarrow 2AlH_3 \quad (3)$$

Mechanochemical method is a well-known technique, which is green and sustainable and offers several economic benefits [53]. It was demonstrated by several groups that this process can be solvent-free and consumes less energy comparing to solvent-based reactions [54,55]. Thus, mechanochemical method is gaining attention as an alternative to conventional solution-based processes and was proposed to synthesize metal hydrides by solid-state reactions with ball milling [53–58]. For example, Fernandez studied milling processes of $LiAlH_4$ with different metal halides (VCl_3, VBr_3 and $AlCl_3$) and observed AlH_3 formation by a mechanochemical reaction between $LiAlH_4$ and $AlCl_3$ [59]. To date, mechanochemical milling has been successfully used for the solid-state synthesis of AlH_3 [40,60–63]. Mechanochemical method for AlD_3 synthesis was employed by Brinks [40]. AlD_3 mixture of various polymorphs was synthesized by mechanically-assisted reaction between $LiAlD_4$ and $AlCl_3$ at 77 K and room temperature (see Eq. (4)) [36].

$$3LiAlD_{4(s)} + AlCl_{3(s)} \rightarrow 4AlD_3 + 3LiCl \quad (4)$$

Lately, Paskevicius obtained a mixture of several polymorphs of AlH_3 (α-, α'-, and γ) by a mechanochemical reaction of $LiAlH_4$ and $AlCl_3$ [61]. The final crystalline size of AlH_3 was 15–17 nm. Sartori reported that the yield of $(\alpha+\alpha')$-AlH_3 increased from 6.1–49.9 mol% when $NaAlH_4 + AlCl_3$ and $LiAlD_4 + AlBr_3$ were used as reagents (see Eqs. (5) and (6)) [62,63]:

$$3LiAlD_4 + AlBr_3 \rightarrow 4AlD_3 + 3LiBr \quad (5)$$

$$3NaAlH_4 + AlCl_3 \rightarrow 4AlH_3 + 3NaCl \quad (6)$$

Prior studies mainly focused on mechanochemical method for AlH_3 composite synthesis rather than the selective synthesis of certain polymorphs during mechanochemically activated reaction process.

Ti and its halides are well-known as effective catalysts for the synthesis of various hydrides. However, most of previous research focused on the effect of Ti-based additives on hydrogen sorption or desorption properties on/from the hydrogen storage materials. For example, Ma demonstrated that presence TiF_3 significantly enhanced dehydrogenation of MgH_2 [64]. Ismail confirmed catalytic role of Ti-containing compounds for performance of $NaAlH_4$-TiF_3 system and promotes dehydrogenation of $NaAlH_4$ [65]. Balema [66,67] recently demonstrated synthesis of Li_3AlH_6 using solid state reaction at ambient temperatures, which proceeded faster with addition of $TiCl_4$. Moreover, Sartori [63] added FeF_3 to the cryomilled $LiAlD_4/AlCl_3$ mixture to accelerate nucleation of the as-milled product and alter its α/α'-AlH_3 ratio. This could be attributed to the isostructure between FeF_3 and α'-AlH_3 which may lead to larger amount of α'-AlH_3 in the as-milled product [63]. Because TiF_3 and α-AlH_3 have similar structure [68], it is possible that fine TiF_3 crystals may act as nucleation seeds for α-AlH_3 formation.

In this work, we studied formation of α-AlH_3 by the mechanochemical process. We used solid-state reaction to obtain AlH_3 by milling using cheaper $AlCl_3$ and metal hydrides as starting materials. Without solvent addition, the separation is omitted and the cost of production can be reduced effectively. We introduced TiF_3 into $LiH/AlCl_3$ reaction system to facilitate nucleation of α-AlH_3. This preliminary finding demonstrates that the usage of TiF_3 during mechanochemical process may be beneficial to the formation of nano-sized α-AlH_3. This simple and efficient synthesis of α-AlH_3 for the first time offers a complete suppression of the parasitic formation of metallic Al. Moreover, the high selectivity of form makes it convenient for further extraction. Meanwhile we systematically studied effect of TiF_3 on the ball-milling assisted reaction rates as well as the underlying mechanisms of the TiF_3-assisted nucleation of α-AlH_3.

2. Experimental

The Gibbs free energy of the reaction between LiH and $AlCl_3$ with a range of 273–380 K is also shown in Fig. S1. The calculation of Gibbs free energy has been described in detail elsewhere [69]. The Gibbs free energy for the reaction (Eq. (7)) at 298 K is about −269 kJ/mol, and therefore the reaction can proceed at room temperature.

$$3\ LiH + AlCl_3 \rightarrow AlH_3 + 3LiCl \tag{7}$$

The starting materials LiH (97%), $AlCl_3$ (99%) and TiF_3 (98%) were purchased from Sigma Aldrich for synthesis of α-AlH_3 composite. The materials, LiH, $AlCl_3$ and TiF_3 were used as-received for this research. The materials were analyzed shortly prior to the use. Purity of materials can be seen from Fig. S2 in ESI. Because of potential sensitivity to moisture, reagents were handled and stored in sealed vials in Ar-filled glove box. Oxygen and water levels in a glove box were > 5 ppm. In an Ar-filled glove box, the reagents, LiH/$AlCl_3$ as well as TiF_3 were weighed and mixed in the various molar ratios firstly. The mixtures were subsequently sealed in a high-pressure ball milling canister for use. Ambient temperature milling was performed using planetary QM-SP4 mixer containing custom-built high-pressure 500 cm^3 stainless steel (316) canister [69–72]. Each canister was sealed on both ends using an o-ring. Milling balls were made from stainless steel 316. The containers were evacuated and filled with H_2 or Ar to a designated pressure ranging between 5 and 40 MPa. Different ranges of milling parameters, such as ball to powder mass ratio, milling speed and gas pressure, were explored to obtain different reaction products. Thus, ball milling was performed for variable durations with different speeds between 100 and 400 rpm. Ball to powder weight ratios were 40:1, 80:1, 120:1 and 200:1. To ensure that average temperatures in the milling vials were close to room temperature, the milling procedure involved alternating milling directions every 20 min. Between every 20 min the milling was discontinued for 10 min. After completion of the mechanochemical reaction, the as-milled product was obtained and collected from vials for further analysis.

For the isothermal desorption measurements, the as-milled samples were loaded into a stainless holder and sealed in an Argon-atmosphere glove box. The hydrogen desorption experiments were carried out in a vacuum apparatus, from which the temperature range from 25 °C to the specified temperature at a vacuum up to 1×10^{-2} Pa. To investigate the dehydriding property of α-AlH_3 composite, the as-milled products were heated in a vacuum chamber from room temperature to different temperatures (80, 120, 140 and 160 °C). The time required for the full dehydriding reaction was fixed within 6500 s, respectively. Once the amounts of hydrogen decomposed from the composite were measured, the vial vacuum change in chamber can be calculated, the corresponding the contents of AlH_3 in its composite could be obtained according to the ideal gas equation as well as stoichiometric weight of AlH_3 calculated by the chemical reaction.

The samples for X-ray diffraction (XRD), scanning electron microscopy (SEM) and solid-state NMR were also prepared in the glove box. The powder X-ray diffraction patterns were obtained by a Philips X'PERT diffractometer equipped with graphite monochromator with a rotating anode tube and operated with Cu Ka radiation source. The voltage and tube current were 45 kV and 40 mA. The samples were scanned from 10 to 90° at 0.5°/min. The average grain size of the α-AlH_3 in the composite was obtained by XRD analysis and the following Scherrer formula.

$$D = \frac{k\lambda}{\beta\cos\theta} \tag{8}$$

Where D is the average grain size, k a constant of 0.89, λ and β the X-ray wavelength and the half-width, θ the diffraction angle.

The as-milled product was placed on carbon tape, coated with a thin layer of gold (Au) by sputtering (EMITECH K450X) and then observed on a scanning electron microscope (SEM, Quanta 200 FEG). The solid-state NMR spectra were collected with a Bruker Avance NMR spectrometer, equipped with a wide bore 14.1 T magnet and a magic angle spinning probe head for rotors of 2.5 mm diameter. To protect the samples from moisture, all samples were packed into a 2.5 mm ZrO_2 rotor and sealed with a tight fitting kel-F cap. NMR shifts were reported in parts per million (ppm). Moreover, this shift was referenced externally with potassium alum to −0.033 ppm, and recycle delay for ^{27}Al was set to 3 s. TEM was conducted on a Tecnai G2 F30 instrument operating at 200 kV. Differential thermal analysis measurements were performed using a TG-DSC METTLER TOLEDO instruments, the samples were handled and transferred to the instrument in T-zero pans and were heated from 40 to 240 °C.

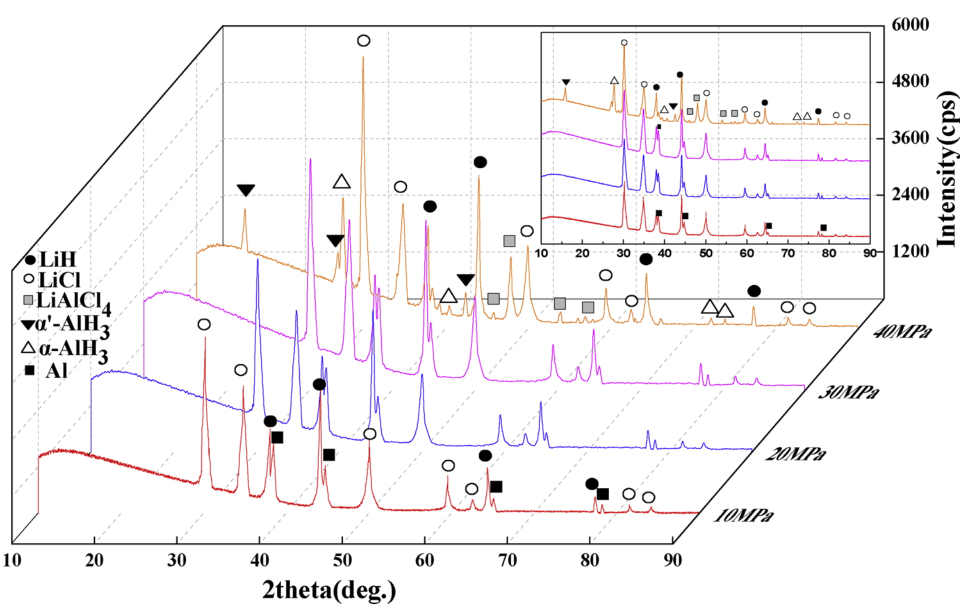

Fig. 1. XRD patterns of LiH and $AlCl_3$ with a molar ratio of 3:1 milled in various hydrogen pressures for 1 h. BPR and rotation speed were 120:1 and 300 rpm.

3. Results and discussion

3.1. Mechanochemical synthesis

Solid-state mechanochemical reaction of Li hydride and $AlCl_3$ is regarded as a green pathway for producing adduct-free AlH_3 [7,20,61]. Brinks reported that ball milling mixture of $LiAlH_4$ and $AlCl_3$ generates mainly Al and LiCl, with small amounts of α-AlH_3 and α′-AlH_3 [40,41]. Gupta et al. [20] suggested that gas pressure affects decomposition of the metastable hydrides into the metal and hydrogen under the mechanochemical conditions. To prevent AlH_3 from decomposing during the ball milling and to find an efficient and cost-effective mechanochemical process for α-AlH_3 synthesis, we conducted LiH/$AlCl_3$ reaction under various hydrogen pressures. Fig. 1 shows XRD patterns of the LiH and $AlCl_3$ mixture (with a 3:1 M ratio) milled for 1 h at various hydrogen pressures. Ball-to-powder weight ratio (BPR) and rotation speed were 120:1 and 300 rpm, respectively. LiH/$AlCl_3$ mixture milled under 10 MPa of hydrogen pressure demonstrated only XRD peaks belonging to the metallic Al, LiCl and unreacted LiH. Thus, the following reaction occurred during the ball milling Eq. (9):

$$3LiH + AlCl_3 \rightarrow 3LiCl + Al + 1.5H_2 \quad (9)$$

Under higher hydrogen pressures, AlH_3 XRD peaks were not observed as well. These results are consistent with the ones obtained by Hlova [7], who also found that replacing AlH_3 with metallic Al resulted in LiH and $AlCl_3$ during ball-milling under 30 MPa hydrogen pressure. Paskevicius elaborated that high-energy milling at room temperature might be needed for AlH_3 dehydrogenation [61]. Although local temperatures are often quite high during high-energy ball milling, such temperature spikes are generally very brief. Moreover, each vial has enough time to cool down during paused milling cycles. Considering kinetic stabilization of AlH_3 at room temperature, raising temperature by a few degrees should not decompose AlH_3. The final product obtained after 1 h milling under 40 MPa of hydrogen pressure was light grey in color and consisted of α- and α′-AlH_3 as well as LiCl, LiH and $LiAlCl_4$ with no metallic Al. Grain sizes of α and α′ AlH_3 phases were up to 83 and 87 nm, respectively. Thus, we conclude that α and α′-AlH_3 phases transformed into their corresponding nano-crystalline forms.

To explore whether the milling parameters, especially milling intensity, were related to the formation of metallic Al, we decreased rotation speed from 300 to 100 rpm. BPR was also reduced from 120:1 to 40:1. The hydrogen pressure was set at 10 MPa. Fig. 2 shows the XRD patterns of products synthesized by milling LiH/LiCl mixture with various ratios for 1 h. At 300 rpm and 80:1 ratio, intensities of LiH and $AlCl_3$ XRD peaks are bigger, suggesting a lower reaction rate. However, metallic Al was formed in these as-milled samples. As the ratio was further reduced to 40:1, diffraction peaks of LiH and $AlCl_3$ were observed. Complete reaction of LiH and $AlCl_3$ with metallic Al as a product was not achieved during the final milling stage. Fig. S3 shows XRD results of the as-milled LiH/LiCl mixture milled at various rotation speeds with the same milling time. The results were the same as shown in Fig. 2: only Al, LiCl, unreacted LiH and $AlCl_3$ diffraction peaks were observed. Although the rotation speed and the BPR have large impacts on the kinetics of the reaction, these parameters cannot suppress formation of metallic Al during mechanochemical reaction between LiH and $AlCl_3$ under a lower hydrogen pressure at room temperature. Thus, pressure is more influential on the mechanochemical synthesis of AlH_3 than milling intensity. Therefore, control of the reaction by changing the pressure during the reaction may be feasible to obtain pure phase of AlH_3.

Despite the fact that hydrogen pressure has such a dramatic influence on the mechanochemical reaction outcome, pressure applied in this work was too high to be used in large-scale AlH_3 production. Mechanically activated solid-gas reactions were studied by several groups [73–76], and many of them confirmed that no gas-solid exchanges occur during mechanochemical reaction of $LiAlH_4$/$AlCl_3$ [61], $NaAlH_4$/$AlCl_3$ and LiH/$AlCl_3$ [7,62,63]. Thus, mechanochemical reaction of the LiH/$AlCl_3$ mixture can also be performed in other inert atmospheres, such as Ar. Therefore, we performed mechanochemical reaction between LiH and $AlCl_3$ (the molar ratio is 3:1) at 300 rpm with BPR of 120:1 for 1 h under various Ar pressures. XRD patterns of the products are very similar to those prepared by milling the LiH/$AlCl_3$ mixture under 10–30 MPa hydrogen pressure (Fig. 3). XRD peaks attributable to metallic Al were observed in samples milled in Ar at 5 MPa. When Ar pressure was 10 MPa, in contrast to the mechanochemical reaction under H_2, unreacted LiH, α, α′-AlH_3, LiCl and $LiAlCl_4$ instead of metallic Al were observed. Thus, pressure is a critical factor that efficiently suppresses formation of Al during the ball milling of LiH/$AlCl_3$ mixture. The value of the critical pressure decreases as the gas molecular weight increases, demonstrating that the critical pressure is related to the physical properties of the ambient atmosphere. During the mechanochemical reaction in the LiH-$AlCl_3$ system at 10–15 MPa, the reaction process did not accelerate based on the XRD results. Complete reaction of LiH and $AlCl_3$ was not achieved by milling the

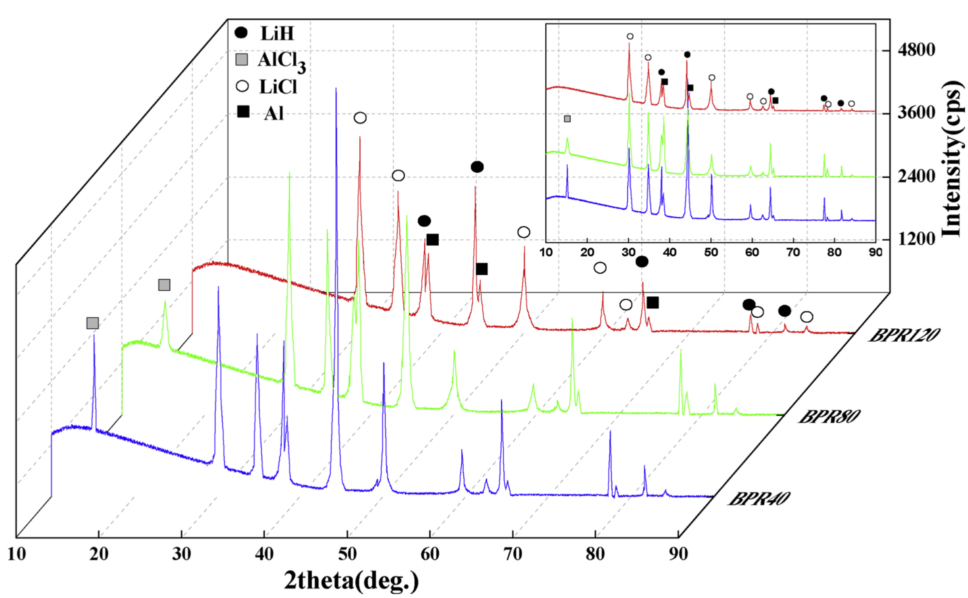

Fig. 2. XRD patterns of LiH and $AlCl_3$ with a molar ratio of 3:1 milled at 300 rpm with various BPR for 1 h. The hydrogen pressure was 10 MPa.

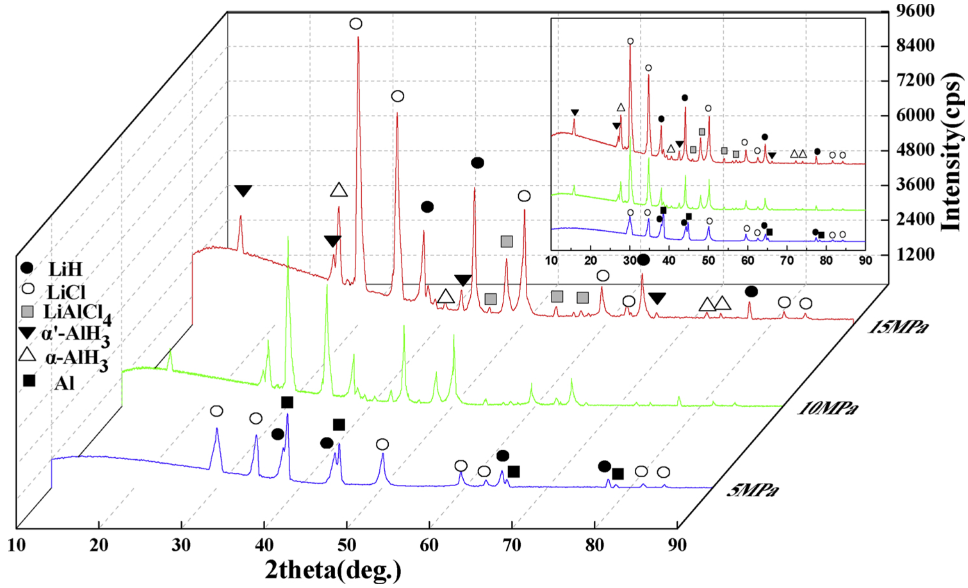

Fig. 3. XRD patterns of LiH and $AlCl_3$ with a molar ratio of 3:1 milled at various Ar pressures for 1 h with a BPR of 120. The rotation speed is 300 rpm.

mixture for 1 h, where unreacted LiH was observed in the final milled product. Therefore, this serves as evidence that the increment in critical pressure is not important to obtain a lower reaction rate, which is more likely controlled by the milling intensity.

It was demonstrated by several groups that the rotation speed and BPR are important parameters in the mechanochemical process. They effectively enhances the chemical reactivity between the reagents, increase the kinetics of the reaction and deduce the time of reaction [7,20,69]. To accelerate mechanochemical reaction of LiH/$AlCl_3$ and obtain AlH_3 composite in a short milling time, the LiH/$AlCl_3$ mixture (the molar ratio is 3:1) was milled at 400 rpm with a BPR 200:1 in Ar at 10 MPa with different milling times. When milling time was 0.5 h, LiH and $AlCl_3$ XRD peaks disappeared (see Fig. 4), indicating acceleration of the mechanochemical reaction rate as the milling intensity increased. Additionally, peaks attributable to $LiAlCl_4$ and α- and α'- AlH_3 phase were observed in the sample milled for 1 h. Thus, a complete reaction with the formation of α-AlH_3 was not achieved. Phases observed after 3 h milling were the same as those obtained by milling LiH/$AlCl_3$ mixture for 1 h but intensity of AlH_3 peaks increases with milling time. Upon milling for 5 h, diffraction peaks of the intermediate $LiAlCl_4$ were still observed. However, its peak between 10° and 20° broadened significantly, indicating formation of an amorphous intermediate compound. Although the BPR and rotation speed accelerate reaction kinetics, it is difficult for LiH/$AlCl_3$ mixture to form AlH_3 nano-composite within 5 h of the mechanochemical reaction. Based on calculation, the average grain size of α-AlH_3 can get 124 nm. Thus, it was ineffective to achieve a complete reaction to generate AlH_3 by increasing reaction intensity. Moreover, formation of different polymorphs of AlH_3 will ultimately lead to the complexity of the hydrogen extraction. This mechanochemical method is considered environmentally friendly because no solvents were used during the whole milling process. This method, involving a addition of $AlCl_3$ into LiH, is a simple way to synthesize α-AlH_3 nano-composite. This method may not be fully applicable to the LiH-$AlCl_3$ system, which was confirmed by our in-depth investigation on formation of α-AlH_3 during short milling periods.

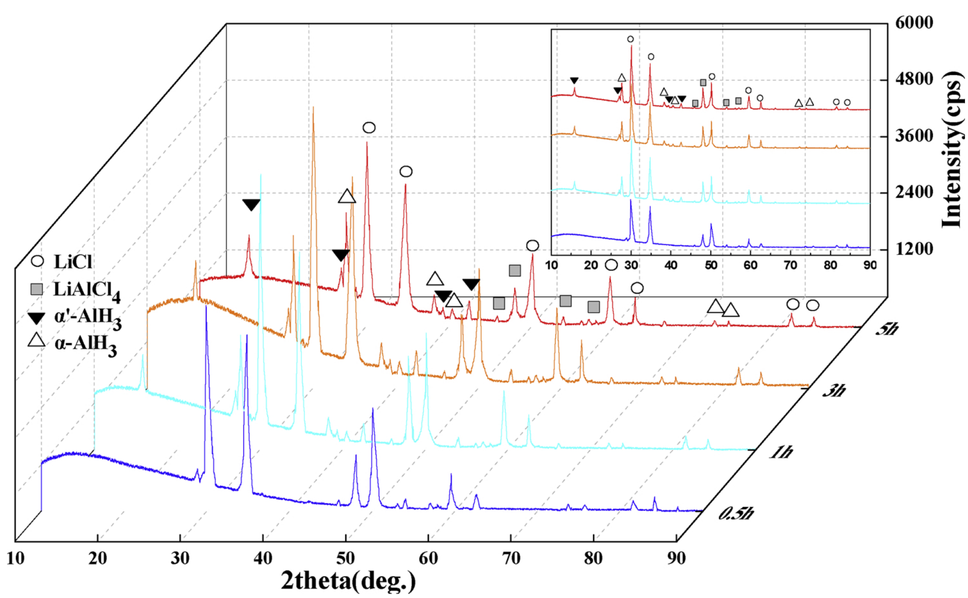

Fig. 4. XRD patterns of the LiH and $AlCl_3$ with a molar ratio of 3:1 milled at 400 rpm with a BPR 200:1 in Ar at 10 MPa for different milling times.

3.2. Effect of TiF_3 on mechanochemical reaction

Sartori demonstrated that FeF_3 not only accelerated nucleation of the as-milled metal hydride [63], but also affected crystalline structure during cryo-milling processes. TiF_3 can act as a seed crystal for formation of α-AlH_3. To investigate the influence of TiF_3 effect on the reaction rate of the mechanochemical reaction of the LiH/$AlCl_3$ mixture and crystallization of the AlH_3 more clearly, we studied XRD patterns of products of mechanochemical reactions of the LiH/$AlCl_3$ mixtures with the presence of the TiF_3 powder at a 3:1:0.1 M ratio milled at 400 rpm with a BPR 200:1 in Ar at 10 MPa for 0.5, 1, 3 and 5 h (see Fig. 5). After milling for 0.5 h, LiH and $AlCl_3$ XRD peaks disappeared, however, complete conversion of the LiH/$AlCl_3$ mixture into AlH_3 and LiCl phases did not occur. Similar diffraction peaks were observed when TiF_3 was not added. Thus, TiF_3 could not accelerate diffusion rate between LiH and $AlCl_3$ after 0.5 h of ball-milling. XRD pattern of the LiH/$AlCl_3$ mixture after milling for 1 h contained $LiAlCl_4$ and α-AlH_3 peaks (Fig. 5), indicating that crystallization of amorphous phases (formed during the first 30 min of ball-milling) occurred within the second 30 min. Thus, TiF_3 can induce quick crystallization of the product from the amorphous phases resulting in α-AlH_3 phase. After ball-milling for 3 h, diffraction peaks of the intermediate phases, such as $LiAlCl_4$, disappeared, leaving only α-AlH_3 and LiCl phases in the final product. As the milling time was increased to 5 h, no substantial changes in the XRD patterns were observed comparing to the products obtained after 3 h milling. However, peak intensity at ˜30° decreased suggesting formation of nano-sized α-AlH_3. The average grain size of α-AlH_3 formed after 5 h milling with the presence of TiF_3 was up to 45 nm. Thus, TiF_3 addition into the LiH/$AlCl_3$ mixture can induce nano-sized α-AlH_3 formation with much smaller crystallite size than without TiF_3. Crystallization rate and selective formation of only α-AlH_3 polymorph occurs because of the synergetic mechanism.

3.3. Analysis of the mechanochemical process

To better understand the mechanochemical process, LiH/$AlCl_3$/TiF_3 mixtures (molar ratio 3:1:0.1) milled at 400 rpm with a BPR of 200:1 for various times were analyzed by SEM (Fig. 6). Milling for 0.5 h did not reduce particle sizes (Fig. 6a). Moreover, a large amount of agglomerates formed with irregular shapes, which can be attributed to the brittleness of the rods. Average particle size of the mixture milled for 0.5 h was ˜40 µm. After 1 h milling, significant amount of large agglomerates were still present (Fig. 6b and c), with finer individual particles adhered to the agglomerates. After 3 h milling, only fine particles were observed with no agglomerates. With longer milling time, the powders became granular in shape with uniform size distribution. The average particle size of the sample milled for 5 h is smaller than 1 µm, which is in agreement with the XRD analysis.

We also analyzed milled samples by ^{27}Al NMR (Fig. 7). Hlova et al. observed an NMR peak centered at ˜ −2 ppm for the mixtures milled for 8 h [7]. They attributed this peak to $AlCl_3$. However, we observed no $AlCl_3$, likely because $AlCl_3$ was consumed after 0.5 h of milling (Fig. 7a). Instead, we observed a dominant spectral band at ˜95 ppm. It was demonstrated by Hlova that the peak at ˜95 ppm is attributed to the four-coordinated Al [7]. The four-coordinated Al signal may be assigned to a superposition of the central transition powder patterns from $LiAlCl_4$ or $LiAlH_4$. With the above XRD analysis, this band corresponds to the four-coordinated Al in $LiAlCl_4$, which is the intermediate product. The same results were observed using DPMAS spectra obtained by Hlova et al. [7]. These results also agree with our XRD analysis. With 1 h milling, NMR spectrum also confirmed the presence of $LiAlCl_4$ but the peak intensity was smaller. NMR spectrum of sample milled for 1 h exhibited broad peaks around at ˜33 ppm and ˜6 ppm (see Fig. 7b), indicating formation of the 6-coordinated Al. The amorphous intermediate products might have more than one Al species because Li-Al-H and Al-H both have priorities in the formation during the mechanochemical reaction. However, the coordinated Al species in Li-Al-H is different from that in Al-H. Grubisic demonstrated that for the other aluminum hydride clusters such as Al_xH_{x+2} ($3 \le \times \le 8$), the polyhedral structure of Al-H cannot be formed with six polymorphic modifications [77]. Thus, it can be deduced that polymers Al-H_x (x = 1, 2, 3 the coordinated Al species is six polymorphic modification) in an amorphous state was formed during the milling process. After milling for 3 h, $LiAlCl_4$ NMR peak disappeared (Fig. 7c), thus, it is very likely that $LiAlCl_4$ as an intermediate product were entirely consumed in the reaction. Additionally, peak corresponding to the 6-coordinated Al changed significantly, which was due to the phase conversion of the intermediate products during extended milling. Thus, NMR can be used as an indicator of the mechanochemical reaction termination. Humphries and Hwang associated the resonance bands at ˜6.0 ppm with the α-AlH_3 phase [78,79]. Thus, after milling for only 60 min, only α-AlH_3 was observed in the product. Therefore, TiF_3 induced crystallization of the amorphous phase and accelerated crystallization of the α-AlH_3 phase.

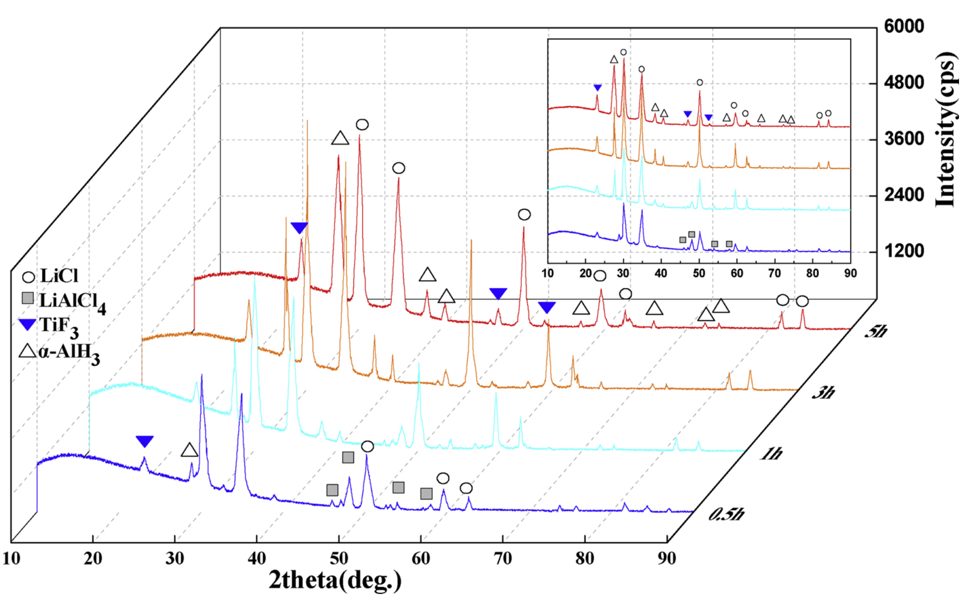

Fig. 5. XRD patterns of the LiH, $AlCl_3$ and TiF_3 with a molar ratio of 3:1:0.1 milled at 400 rpm with a BPR 200:1 in Ar at 10 MPa for different milling times.

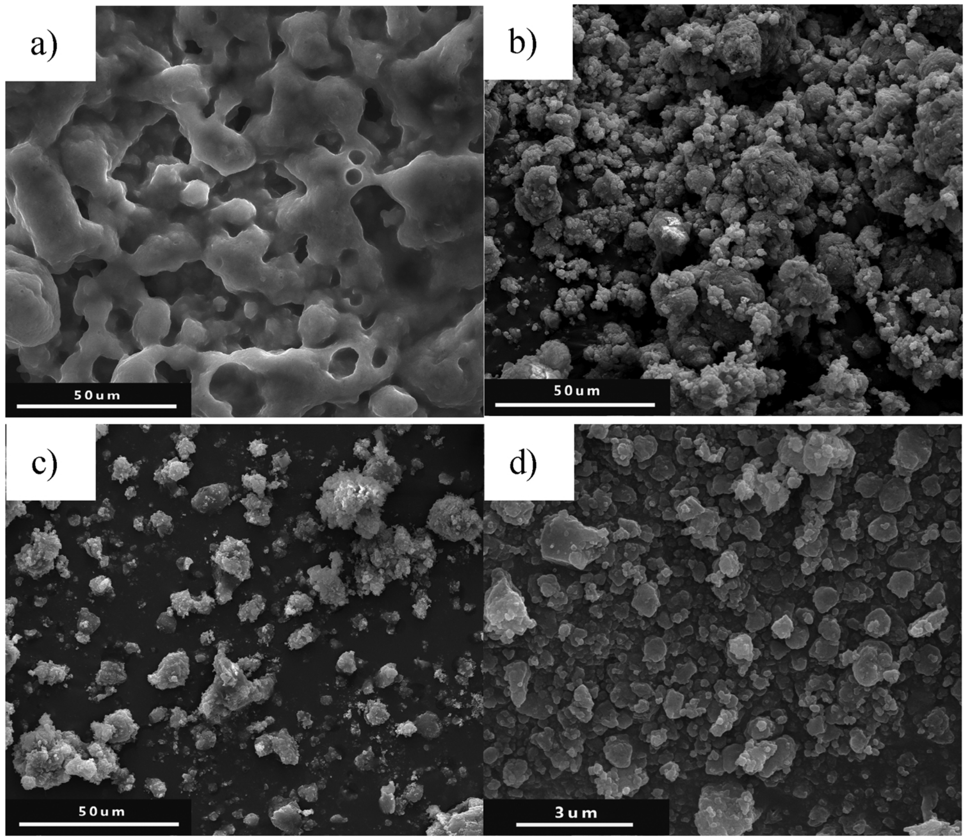

Fig. 6. Morphology of the LiH, $AlCl_3$ and TiF_3 with a molar ratio of 3:1:0.1 milled at 400 rpm with a BPR 200:1 in Ar at 10 MPa for different milling times: (a) 0.5 h, (b) 1 h, (c) 3 h, (d) 5 h.

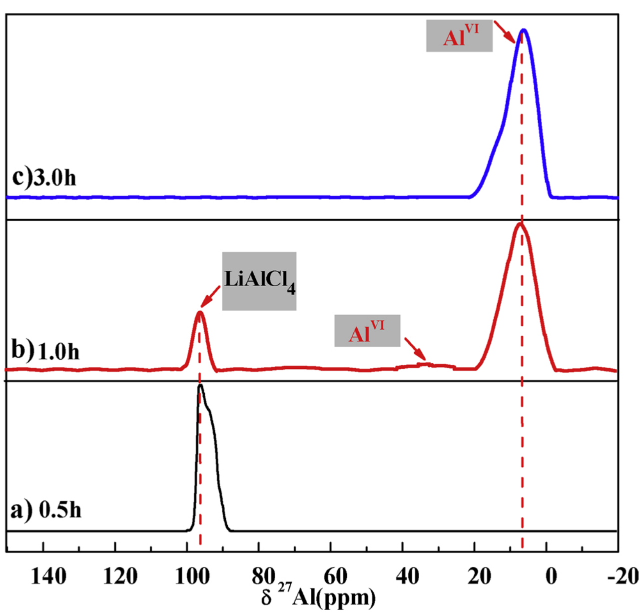

Fig. 7. Solid-state ^{27}Al NMR spectra of the LiH, $AlCl_3$ and TiF_3 with a molar ratio of 3:1:0.1 milled at 400 rpm with a BPR 200:1 in Ar at 10 MPa for the 0.5, 1, 3 h.

3.4. Reaction and synergetic mechanism

Even though we thoroughly analyzed solid-state mechanochemical reaction by XRD and NMR, the actual details of the reaction mechanism and synergistic effect of TiF_3 were still somewhat unclear. Typically, AlH_3/LiCl composite can form directly during the milling process and mechanism of the AlH_3 formation during this process is similar to the one reported by Paskevicius [61,80]. XRD results (Fig. 1) indicated that metallic Al instead of AlH_3 formed during the milling process. To investigate the mechanism for the Al formation during ball milling of LiH/$AlCl_3$, this mechanochemical reaction was controlled by a stepwise reduction of Ar pressure. The as-milled $LiAlCl_4$/LiCl composites comes from 3:1:0.1 LiH:$AlCl_3$:TiF_3 mixture at 400 rpm under a 10 MPa Ar atmosphere, with a BPR of 200:1 for 0.5 h milling conditions were used as the original compounds to be milled at a lower gas pressure. During the second stage milling Ar pressure was reduced to 5 MPa but the other milling parameters remained unchanged. Fig. 8 shows $LiAlCl_4$/LiCl composites milled at 5 MPa for 0.5 and 1 h with the same BPR and the rotation speeds. LiCl remained present, while some of the $LiAlCl_4$ was consumed after 30 min, based on the lower intensities of peaks at ˜29° and ˜48°. New peaks, corresponding to the metallic Al, appeared at 38 and 40°. Additional 30 min of milling resulted in disappearance of the $LiAlCl_4$ peaks. At the same time, peaks corresponding to metallic Al and LiCl by-products showed high intensities. Thus, this mechanically activated reaction involves formation of $LiAlCl_4$ and amorphous intermediate product, and their subsequent decomposition. Thus, comparing to the decomposition of AlH_3 during the milling, the above experimental evidence indicated that metallic Al formed at lower pressures appeared as a result of the transformation of the $LiAlCl_4$ intermediate products.

It appears that TiF_3 has a synergistic effect on the mechanochemical reaction of LiH and $AlCl_3$. According to the NMR analysis (Fig. 7b), when TiF_3 was added into the reaction system, almost all of the 6-coordinated Al in $AlCl_3$ was converted into the 4-coordinated Al in $LiAlCl_4$ and amorphous Al-H_x (x = 1, 2, 3). With furthermore milling, $LiAlCl_4$ and amorphous Al-H_x were first converted to amorphous but then to the 6-coordinated Al in α-AlH_3. The intermediate $LiAlCl_4$ and amorphous Al-H_x were identified by both XRD and NMR, while, its role in the

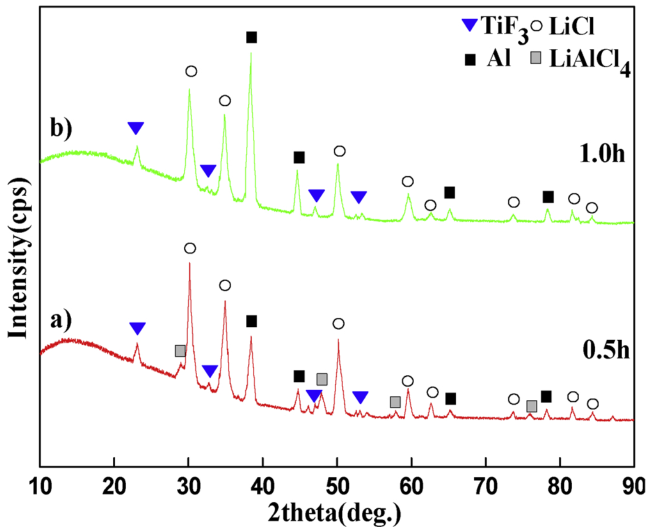

Fig. 8. XRD patterns of $LiAlCl_4$/LiCl composites milled at 400 rpm and 5 MPa Ar pressure with a BPR of 200:1 for different times: a) 0.5 h, b) 1 h. The as-milled $LiAlCl_4$/LiCl composites comes from 3:1:0.1 LiH:$AlCl_3$:TiF_3 mixture at 10 MPa Ar pressure with the same BPR and the rotational speeds for 0.5 h milling conditions.

mechanochemical process still remains unclear. Ashby et al. [81,82] demonstrated that the transformation between Al^{IV} and Al^{VI} species may occur as a result of Cl replacement by H in $LiAlCl_4$, which leads to $LiAlCl_{4-x}H_x$ (x = 1, 2, 3) formation. Thus, it is assumed that a $LiAlCl_{4-x}H_x$ amorphous intermediate formed during the furthermore milling of $LiAlCl_4$ and Al-H_x. It is very likely that $LiAlCl_{4-x}H_x$ amorphous intermediate species are unstable during the ball milling. Compared with more stable α-AlH_3, this intermediate product cannot maintain its crystalline state during the extended milling times. Therefore, this $LiAlCl_{4-x}H_x$ intermediate eventually transforms into α-AlH_3. TiF_3 was introduced into the reaction system to shorten transformation time of the amorphous intermediate phases into α-AlH_3 phase. The fine TiF_3 might act as seed crystals and accelerate substitution of the Cl by H in $LiAlCl_{4-x}H_x$. Moreover, because of the isostructuralism of TiF_3 and α-AlH_3, TiF_3 prompts α-AlH_3 formation during a short milling time. Thus, an intermediate amorphous $LiAlCl_{4-x}H_x$ phase formed during the milling process. By introducing TiF_3, this intermediate phase can be crystallized easily. All Al atoms in the final α-AlH_3 phase are six-coordinated with hydrogen atoms. The mechanism of this mechanochemical reaction can be described according to Eq. (10).

$$3LiH + AlCl_3 \rightarrow LiAlCl_4 + AlH_x + 2LiCl \rightarrow LiAlCl_{4-x}H_x + 2LiCl \rightarrow 3LiCl + \alpha\text{-}AlH_3 \quad (10)$$

3.5. Dehydrogenation properties of the α-AlH_3 nano-composite

Considering the influence of Ti-based additives on the desorption properties of hydrogen storage materials, the α-AlH_3/LiCl nano-composite with TiF_3 might have different dehydriding behavior than pure AlH_3. Thus, we studied dehydriding properties of TiF_3-doped α-AlH_3/LiCl nano-composite under isothermal conditions in the temperature range 80–160 °C. Amount of H_2 released from the composite was obtained by dividing actual H_2 content by the stoichiometric AlH_3 weight. As shown in Fig. 9, isothermal dehydriding curves exhibit sigmoidal features with distinct introduction, acceleration and decay periods. This behavior is similar to decomposition of other comparable materials. Compared with α-AlH_3/LiCl nano-composite obtained without TiF_3 (inserting in the Fig. 9), additive TiF_3 accelerated decomposition kinetics of α-AlH_3/LiCl nano-composite. Additionally, desorption kinetics improved as the temperature was increased to 160 °C. Thus, temperature can have a large impact on the dehydrogenation reaction kinetics of α-AlH_3/LiCl composite. The reaction of AlH_3 dehydrogenation can be expressed in Eq. (11):

$$2AlH_3 \rightarrow 2Al + 3H_2\uparrow \quad (11)$$

As the reaction temperature increased from 80 to 120 °C, the time of full decomposition decreased rapidly, that a complete decomposition was obtained within 3000 s, suggesting significantly higher decomposition rate at higher temperature (see the Fig. 9). In comparison, only 8.0 wt% of H_2 was released at 20–160 °C during α-AlH_3 decomposition reported by Chen [83]. After we annealed our as-milled α-AlH_3 at 140 °C, the shape of the dehydriding curve became step-wise for 1160 s with the same hydrogen amount as at 120 °C. Graetz reported that full decomposition time for α-AlH_3 at 138 °C could be achieved within 1800s [84]. After we annealed our composite at 160 °C, decomposition curve in Fig. 9 was also step-wise for 750 s with higher hydrogen content equal to 9.92 wt%. Shahi found that among all Ti based additives, TiF_3 is found to be the most effective catalyst for dehydrogenation kinetics of nano MgH_2 [85]. However, full decomposition for the MgH_2/TiF_3 at 300 °C could be achieved within 1800s with a maximal hydrogen content of 6.3 wt%. Therefore, TiF_3 not only influenced decomposition temperature of α-AlH_3 but also improved dehydriding kinetics of α-AlH_3. Although numerous papers showing a dehydriding rate enhancement with the addition of transition metal additives in AlH_3 [86,87], the excess transition metal additives have little influence on the dehydriding property of AlH_3. The α-AlH_3/LiCl nano-composite with different amounts of TiF_3 (molar ration of LiH/$AlCl_3$/TiF_3 are 3:1:0.1, 3:1:0.2, 3:1:0.3) were heated at 160 °C for different times. As shown in Fig. S4, desorption kinetics were improved as the molar ratio of TiF_3 increased. However, increment of TiF_3 results in a relatively small increase in the rate. After we annealed our as-milled α-AlH_3/LiCl/TiF_3 composite at the same temperature, the full dehydriding time of the curve(III) was reduced from 750 s to 570 s.

DSC analysis was performed to further understand the dehydriding process [88,89]. Fig. 10a shows DSC thermograms of as-milled α-AlH_3 composite with TiF_3 at several heating rates(composite synthesized from LiH/$AlCl_3$/TiF_3 with a molar ration of 3:1:0.1). The DSC thermograms contain only one endothermic peak within the range of 40–240 °C. The endothermic peak between 80 and 190 °C corresponds to the dehydriding reaction of the α phase [90]. This result indicates that no new phases formed, and α-AlH_3 does not react with TiF_3 during its dehydrogenation. Based on the above non-isothermal analysis, the dehydriding temperature of α-AlH_3 is remarkably reduced with the TiF_3

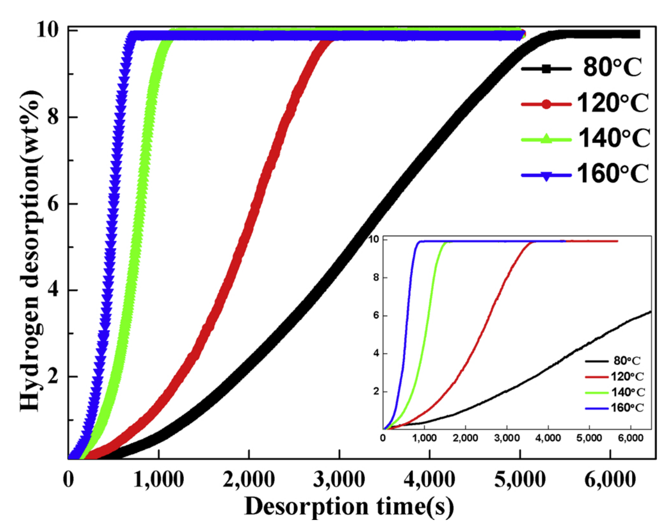

Fig. 9. The dehydriding curves of final α-AlH_3/LiCl/TiF_3 nano-composite at different temperatures. Insert is the dehydriding curves of α-AlH_3/LiCl composite without TiF_3.

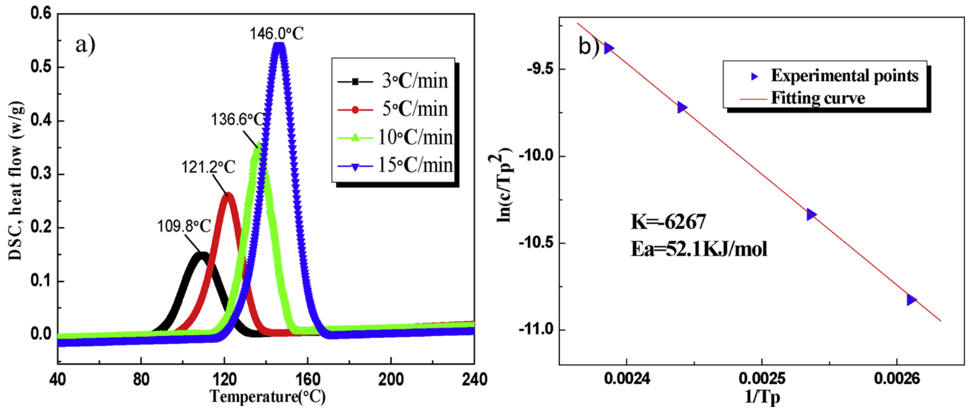

Fig. 10. (a) DSC curves and (b) The Kissinger plot of the α-AlH_3/LiCl/TiF_3 nano-composite doped with TiF_3. Composite synthesized from LiH/$AlCl_3$/$TiF_3$with a molar ration of 3:1:0.1.

in the composite. To determinate the apparent activation energy (Ea) of this process, we studied desorption kinetics of the α-AlH_3/LiCl nano-composite using the Kissinger's method. Moreover, the relationship between the activation energy (Ea, KJ/mol), the heating rate (c, K/min), the gas constant (R, 8.314 J/mol K) and the peak temperature of dehydriding (T_P, K) in the DSC curve is described by following Kissinger's equation:

$$\ln(c/T_p^2) = -(E_a/RT_p)+A \tag{12}$$

E_a for the dehydrogenation reaction calculated from DSC data are shown in Fig. 10b. The E_a for the hydrogen desorption of α-AlH_3 in the composite was 52.1 KJ/mol. This value is significantly lower than the value 104 KJ/mol of the α-AlH_3 without TiF_3 reported by Gabis [91]. It was reported by Nakagawa that with NbF_5 in α-AlH_3, the α-AlH_3/NbF_5 present a quite high hydrogen desorption capacity and fast kinetics. It is worth noting that the activation energy of dehydriding of α-AlH_3 was reduced from 104 to 96 kJ/mol(ΔE is 8 kJ/mol) [92]. Based on above analysis, this decrease in the kinetic barrier contributed to the improvement in the hydrogen desorption kinetics of α-AlH_3/LiCl/TiF_3 nano-composite.

3.6. Microstructural evolution during the dehydriding process

Morphology of the α-AlH_3/LiCl/TiF_3 composite during the dehydriding process was studied with SEM images. Fig. 11 shows the SEM images of product heated at 160 °C for various times. As observed in the Fig. 11a, the particles after desorption for 10 min at 160 °C with a range of 400–500 nm is generally smaller than those of the as-milled α-AlH_3/LiCl/TiF_3 sample, indicating particle refinement of the product during dehydrogenation of AlH_3. When the heating time was increased to 20 min, it is observed form Fig. 11b that the difference in surface morphology is significant due to the aggregation of the composite after further desorption. The morphological characteristics of the product in Fig. 11c, indicate that when heating time was extended to 30 min, the inhomogeneity in particle distributions is significant and most individual particles had an average size between 5–7 μm. This may contribute to the further aggregation of the composite. Based on above SEM observation, it can be seen that the particles in the composite tend to aggregate with the longer heating time. Graetz found that the aggregation of particles will result in the reduction of the gateways for hydrogen diffusion [36]. This can explain the phenomenon that the dehydriding rates of the α-AlH_3/LiCl/TiF_3 composite declined with dehydriding time in the later stage of the isothermal dehydriding process. Thus, particle aggregation may give rise to the decline of the dehydriding kinetics of the α-AlH_3/LiCl/TiF_3 nano-composite.

After the desorption process of the α-AlH_3/LiCl/TiF_3 composite, the phase transformation, structural and morphological changes were not clearly understood. Fig. 12 shows the TEM of the α-AlH_3/LiCl/TiF_3 nano-composite heated at 160 °C for 10 min. A large amount of much finer crystallines are observed from Fig. 12a. The nucleation and quite uniform in size distribution of the crystallites indicates that the dehydrogenation of the α-AlH_3 has occurred simultaneously after heating. This phenomenon has a good agreement with the above dehydriding outcomes. The average size of nano-composite after heating process is approximately to be 50 nm. A selected area diffraction pattern (SADP) of the same material is also shown in Fig. 12b. Lattice fringes confirmed that finer crystalline particles matched Al, LiCl and TiF_3 phases (see Fig. 12b). Lattice spacings equal to 2.34 and 2.02 Å correspond to (111) and (200) planes of metallic Al. Moreover, the typical lattice spacing which is determined to be 1.55, 1.29 and 3.88, 1.94 Å are attributed to the (311) and (400) planes of the LiCl and (012) and (024) planes of the metal TiF_3, respectively. These observations indicated that the α-AlH_3 phase decomposed without reacting with TiF_3, which is in agreement with the DSC results.

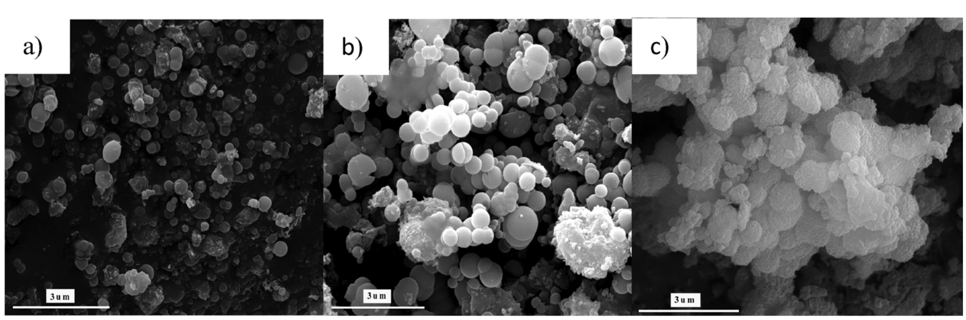

Fig. 11. SEM images of as-milled α-AlH_3/LiCl/TiF_3 nano-composite heated at 160 °C for various times:a) 10 min, b) 20 min, c) 30 min.

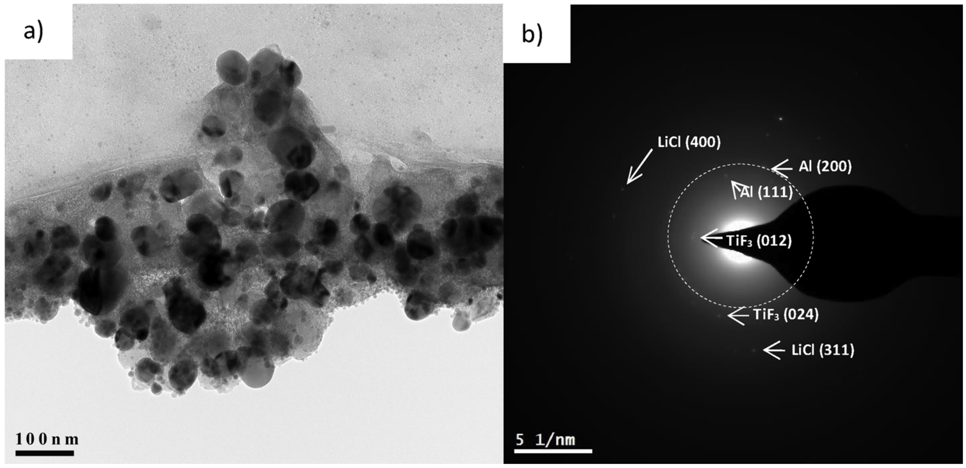

Fig. 12. TEM images of the α-AlH_3/LiCl/TiF_3 nano-composite after dehydriding at 160 °C for 10 min: (a) and (b) are the bright field image and corresponding ED pattern.

4. Conclusions

We demonstrated that milling could be used as a simple and efficient method to prepare nanocrystalline α-AlH_3. The type of gas and the pressure are important for the mechanochemical synthesis of α-AlH_3 nano-composite. Using proper gas and pressures, we were able to entirely suppress formation of metallic Al. When TiF_3 was introduced into the reaction system, LiH and $AlCl_3$ underwent several intermediate stages before the final product - nano-structured α-AlH_3/LiCl was formed. The average grain size of α-AlH_3 nanoparticles embedded in LiCl reached ˜45 nm after milling in Ar for 5 h. TiF_3 has significantly affected dehydriding properties of AlH_3, compared to the α-AlH_3/LiCl nano-composite without TiF_3. The as-milled α-AlH_3/LiCl-TiF_3 composite has a hydrogen desorption of 9.92 wt% at 160 °C within 750 s, which is very close to the theoretical hydrogen capacity of AlH_3. Apparent activation energy of α-AlH_3 hydrogen desorption in the composite was 52.1 KJ/mol with the addition of TiF_3.

Acknowledgements

The present work was supported financially by the Natural Science Foundation of Hebei Province (Grant E2018502054), the National Major Science and Technology Program for Water Pollution Control and Treatment (Grant 2017ZX07101-001-001) and the National Nature Science Foundation of China (Grant 21506043).This work was also supported by the Fundamental Research Funds for the Central Universities (Grant 2017MS141), Opening Project of the Key Laboratory for Green Processing of Chemical Engineering of Xinjiang Bingtuan (KF201702), and Shihezi University 2017 High Level Intelligence Supporting Project (RCSX201731).

Appendix A. Supplementary data

Supplementary material related to this article can be found, in the online version, at doi:https://doi.org/10.1016/j.jhazmat.2019.03.064.

References

[1] G. Landucci, T. Alessandro, C. Valerio, Inherent safety key performance indicators for hydrogen storage systems, J. Hazard. Mater. 159 (2008) 554–566.
[2] J. Zheng, X. Xiao, L. Zhang, Y. He, S. Li, H. Ge, L. Chen, Study on the dehydrogenation properties and reversibility of $Mg(BH_4)_2$-AlH_3 composite under moderate conditions, Int. J. Hydrogen Energy 42 (2017) 8050–8056.
[3] S. Orimo, Y. Nakamori, J.R. Eliseo, A. Züttel, C.M. Jensen, Complex hydrides for hydrogen storage, Chem. Rev. 107 (2007) 4111–4132.
[4] M. Savić, J. Radaković, K. Batalović, Study on electronic properties of α-, β- and γ-AlH_3–The theoretical approach, Comp. Mater. Sci. 134 (2017) 100–108.
[5] L. Wang, Y. Zhang, R. Wang, et al., Advanced monoethanolamine absorption using sulfolane as a phase splitter for CO_2 capture, Environ. Sci. Technol. 52 (2018) 14556–14563.
[6] P. Zhang, X. Tian, D. Fu, CO_2 removal in tray tower by using AAILs activated MDEA aqueous solution, Energy 161 (2018) 1122–1132.
[7] I.Z. Hlova, S. Gupta, J.F. Goldston, T. Kobayashi, M. Pruski, V.K. Pecharsky, Dry mechanochemical synthesis of alane from LiH and $AlCl_3$, Faraday Discuss. 170 (2014) 137–153.
[8] E.G. Bardaji, N. Hanada, O. Zabara, M. Fichtner, Effect of several metal chlorides on the thermal decomposition behaviour of α-$Mg(BH_4)_2$, Int. J. Hydrogen Energy 36 (2011) 12313–12318.
[9] C. Duan, J. Huo, F. Li, M. Yang, H. Xi, Ultrafast room-temperature synthesis of hierarchically porous metal–organic frameworks by a versatile cooperative template strategy, J. Mater. Sci. 53 (2018) 16276–16287.
[10] J. Liu, C. Zhang, L. Xu, S. Ju, Borophene as a promising anode material for sodium-ion batteries with high capacity and high rate capability using DFT, RSC Adv. 8 (2018) 17773–17785.
[11] J. Wang, S. Zhou, Z. Zhang, D. Yurchenko, High-performance piezoelectric wind energy harvester with Y-shaped attachments, Energy Convers. Manage. 181 (2019) 645–652.
[12] J. Liu, X. Lv, J. Li, L. Zhang, J. Peng, Densification and microstructure of magnesium aluminate spinel for adding method of Sc_2O_3, J. Alloys Compd. 735 (2018) 394–399.
[13] K. Wu, K. Du, G. Hu, A novel design concept for fabricating 3D graphene with the assistant of anti-solvent precipitated sulphates and its Li-ion storage properties, J. Mater. Chem. A 6 (2018) 3444–3453.
[14] X. Liu, X. Ma, W. Yuan, et al., Concise chemistry modulation of the SMM behavior within a family of mononuclear Dy (III) complexes, Inorg. Chem. 57 (2018) 14843–14851.
[15] X. Liu, F. Li, X. Ma, P. Cen, et al., Coligand modifications fine-tuned the structure and magnetic properties of two triple-bridged azido-Cu(II) chain compounds exhibiting ferromagnetic ordering and slow relaxation, Dalton Trans. 46 (2017) 1207–1217.
[16] X. Liu, L. Sun, H.L. Zhou, P.P. Cen, X.Y. Jin, G. Xie, S.P. Chen, Q.L. Hu, Single-ion-magnet behavior in a two-dimensional coordination polymer constructed from CoII nodes and a pyridylhydrazone derivative, Inorg. Chem. 54 (2015) 8884–8886.
[17] C. Wolverton, V. Ozoliņš, M. Asta, Hydrogen in aluminum: first-principles calculations of structure and thermodynamics, Phys. Rev. B 69 (2004) 144109.
[18] J. Graetz, J.J. Reilly, Decomposition kinetics of the AlH_3 polymorphs, J. Phys. Chem. B 109 (2005) 22181–22185.
[19] J. Graetz, New approaches to hydrogen storage, Chem. Soc. Rev. 38 (2009) 73–82.
[20] S. Gupta, T. Kobayashi, I.Z. Hlova, J.F. Goldston, M. Pruski, V.K. Pecharsky, Solvent-free mechanochemical synthesis of alane, AlH_3: effect of pressure on the reaction pathway, Green Chem. 16 (2014) 4378–4388.
[21] Y. Nakagawa, S. Isobe, Y. Wang, N. Hashimoto, S. Ohnuki, L. Zeng, L. Shusheng, I. Takayuki, Y. Kojima, Dehydrogenation process of AlH_3 observed by TEM, J. Alloys Compd. 580 (2013) S163–S166.
[22] D.A. Anton, T. Motyka, Arlington (VA)US DOE Hydrogen Program Annual Merit Review Proceedings2014, US DOE Hydrogen Program Annual Merit Review Proceedings (2014) http://www.hydrogen.energy.gov/pdfs/review12/st004_anton_2012_o.pdf, accessed: July.
[23] Y.F. Khalil, Experimental determination of dust cloud combustion parameters of α-AlH_3 powder in its charged and fully discharged states for H_2 storage applications, J. Loss Prevent. Proc. 44 (2016) 334–346.
[24] J.M. Pasini, C. Corgnale, B.A. van Hassel, T. Motyka, S. Kumar, K.L. Simmons, Metal hydride material requirements for automotive hydrogen storage systems, Int. J. Hydrogen Energy 38 (2013) 9755–9765.
[25] H. Li, L. Luo, P. Kunal, et al., Oxygen reduction reaction on classically immiscible bimetallics: a case study of RhAu, J. Phys. Chem. C 122 (2018) 2712–2716.
[26] H. Li, G. Henkelman, Dehydrogenation selectivity of ethanol on close-packed transition metal surfaces: a computational study of monometallic, Pd/Au, and Rh/Au catalysts, J. Phys. Chem. C 121 (2017) 27504–27510.
[27] K. Wang, J.B. Pang, L.W. Li, et al., Synthesis of hydrophobic carbon nanotubes/

reduced graphene oxide composite films by flash light irradiation, Front. Chem. Sci. Eng. 12 (2018) 376–382.

[28] K. Wang, S. Zhou, Y. Zhou, et al., Synthesis of porous carbon by activation method and its electrochemical performance, Int. J. Electrochem. Sci. 13 (2018) 10766–10773.

[29] S. Tang, D. Yuan, Y. Rao, et al., Percarbonate promoted antibiotic decompo- sition in dielectric barrier discharge plasma, J. Hazard. Mater. 366 (2019) 669–676.

[30] N. Li, S. Tang, Y. Rao, et al., Improved dye removal and simultaneous electricity production in a photocatalytic fuel cell coupling with persulfate, Electrochim. Acta 270 (2018) 330–338.

[31] K. Yin, S. Yang, X.R. Dong, D.K. Chu, X. Gong, J.A. Duan, Femtosecond laser fabrication of shape-gradient platform: underwater bubbles continuous self-driven and unidirectional transportation, Appl. Surf. Sci. 471 (2019) 999–1004.

[32] K. Yin, S. Yang, X. Dong, D. Chu, J. Duan, J. He, Robust laser-structured asymmetrical PTFE mesh for underwater directional transportation and continuous collection of gas bubbles, Appl. Phys. Lett. 112 (2018) 243701.

[33] T. Bazyn, R. Eyer, H. Krier, N. Glumac, Combustion characteristics of aluminum hydride at elevated pressure and temperature, J. Propul. Power 20 (2004) 427–431.

[34] R. Zidan, B.L. Garcia-Diaz, C.S. Fewox, A.C. Stowe, J.R. Gray, A.G. Harter, Aluminium hydride: a reversible material for hydrogen storage, Chem. Commun. 25 (2009) 3717–3719.

[35] V. Weiser, N. Eisenreich, A. Koleczko, E. Roth, On the oxidation and combustion of AlH_3 a potential fuel for rocket propellants and gas generators, Propellants Explos. Pyrotech. 32 (2007) 213–221.

[36] J. Graetz, J.J. Reilly, V.A. Yartys, J.P. Maehlen, B.M. Bulychev, V.E. Antonov, B.P. Tarasov, I.E. Gabis, Aluminum hydride as a hydrogen and energy storage material: past, present and future, J. Alloys Compd. 509 (2011) S517–S528.

[37] J. Yang, P.R. Beaumont, T.D. Humphries, Efficient synthesis of an aluminum amidoborane ammoniate, Energies 8 (2015) 9107–9116.

[38] J.W. Turley, H.W. Rinn, Crystal structure of aluminum hydride, Inorg. Chem. 8 (1969) 18–22.

[39] X. Ke, A. Kuwabara, I. Tanaka, Cubic and orthorhombic structures of aluminum hydride AlH_3 predicted by a first-principles study, Phys. Rev. B 71 (2005) 184107.

[40] H.W. Brinks, A. Istad-Lem, B.C. Hauback, Mechanochemical synthesis and crystal structure of α'-AlD_3 and α-AlD_3, J. Phys. Chem. B 110 (2006) 25833–25837.

[41] H.W. Brinks, W. Langley, C.M. Jensen, J. Graetz, J.J. Reilly, B.C. Hauback, Synthesis and crystal structure of β-AlD_3, J. Alloys Compd. 433 (2007) 180–183.

[42] V.A. Yartys, R.V. Denys, J.P. Maehlen, Ch. Frommen, M. Fichtner, B.M. Bulychev, H. Emerich, Double-bridge bonding of aluminium and hydrogen in the crystal structure of γ-AlH_3, Inorg. Chem. 46 (2007) 1051–1055.

[43] O. Stecher, E. Wiberg, Über einen nichtflüchtigen, polymeren aluminiumwasserstoff $(AlH_3)x$ und einige flüchtige verbindungen des monomeren AlH_3, Ber. Dtsch. Chem. Ges. B 75 (1942) 2003.

[44] A.E. Finholt, A.C. Bond, H.I. Schlesinger, Lithium aluminum hydride, aluminum hydride and lithium gallium hydride, and some of their applications in organic and inorganic chemistry1, J. Am. Chem. Soc. 69 (1947) 1199–1203.

[45] G. Chizinsky, G.G. Evans, T.R.P. Gibb, M.J. Rice, Non-solvated aluminum hydride, J. Am. Chem. Soc. 77 (1955) 3164–3165.

[46] E.C. Ashby, The direct synthesis of amine alanes, J. Am. Chem. Soc. 86 (1964) 1882–1883.

[47] F.M. Brower, N.E. Matzek, P.F. Reigler, H.W. Rinn, C.B. Roberts, D.L. Schmidt, Preparation and properties of aluminum hydride, J. Am. Chem. Soc. 98 (1976) 2450–2453.

[48] B.M. Bulychev, V.N. Verbetskii, A.I. Sizov, Non-solvated aluminum hydride. Crystallization from diethyl ether-benzene solutions, Russ. Chem. Bull. 56 (2007) 1305–1312.

[49] B.M. Bulychev, V.N. Verbetskii, P.A. Storozhenko, Direct synthesis of unsolvated aluminum hydride involving Lewis and Bronsted acids, Russ. J. Inorg. Chem. 53 (2008) 1000–1005.

[50] T. Kraus, M. Scardera, Preparation of AlH3 via NaAlH4-AlCl3 in ether-toluene. (1974) U.S. Patent No. 3,857,930.

[51] H. Saitoh, A. Machida, Y. Katayama, K. Aoki, Formation and decomposition of AlH_3 in the aluminum-hydrogen system, Appl. Phys. Lett. 93 (2008) 151918.

[52] H. Saitoh, A. Machida, Y. Katayama, K. Aoki, Hydrogenation of passivated aluminum with hydrogen fluid, Appl. Phys. Lett. 94 (2009) 151915.

[53] V. Birke, J. Mattik, D. Runne, Mechanochemical reductive dehalogenation of hazardous polyhalogenated contaminants, J. Mater. Sci. 39 (2004) 5111–5116.

[54] F. Sun, Y. Yao, X. Li, The heat and mass transfer characteristics of superheated steam coupled with non-condensing gases in horizontal wells with multi-point injection technique, Energy 143 (2018) 995–1005.

[55] B.I. Park, S. Yu, Y. Hwang, Highly crystalline Fe_2GeS_4 nanocrystals: green synthesis and their structural and optical characterization, J. Mater. Chem. A 3 (2015) 2265–2270.

[56] Y. Kim, E.K. Lee, J.H. Shim, Y.W. Cho, K.B. Yoon, Mechanochemical synthesis and thermal decomposition of $Mg(AlH_4)_2$, J. Alloys Compd. 422 (2006) 283–287.

[57] R.A. Varin, C. Chiu, T. Czujko, Z. Wronski, Mechano-chemical activation synthesis (MCAS) of nanocrystalline magnesium alanate hydride $[Mg(AlH_4)_2]$ and its hydrogen desorption properties, J. Alloys Compd. 439 (2007) 302–311.

[58] K.T. Møller, J.B. Grinderslev, T.R. Jensen, A $NaAlH_4$-$Ca(BH_4)_2$ composite system for hydrogen storage, J. Alloys Compd. 720 (2017) 497–501.

[59] J.A. Fernandez, F. Aguey-Zinsou, M. Elsaesser, X.Z. Ma, M. Dornheim, T. Klassen, R. Bormann, Mechanical and thermal decomposition of $LiAlH_4$ with metal halides, Int. J. Hydrogen Energy 32 (2007) 1033–1040.

[60] J. Huot, D.B. Ravnsbæk, J. Zhang, F. Cuevas, M. Latroche, T.R. Jensen, Mechanochemical synthesis of hydrogen storage materials, Prog. Mater. Sci. 58 (2013) 30–75.

[61] M. Paskevicius, D.A. Sheppard, C.E. Buckley, Characterisation of mechanochemically synthesised alane (AlH_3) nanoparticles, J. Alloys Compd. 487 (2009) 370–376.

[62] S. Sartori, S.M. Opalka, O.M. Løvvik, M.N. Guzik, X. Tang, B.C. Hauback, Experimental studies of α-AlD_3 and α′-AlD_3 versus first-principles modelling of the alane isomorphs, J. Mater. Chem. 18 (2008) 2361–2370.

[63] S. Sartori, A. Istad-Lem, H.W. Brinks, B.C. Hauback, Mechanochemical synthesis of alane, Int. J. Hydrogen Energy 34 (2009) 6350–6356.

[64] M. Ismail, Y. Zhao, X.B. Yu, S.X. Dou, Improved hydrogen storage performance of MgH_2–$NaAlH_4$ composite by addition of TiF_3, Int. J. Hydrogen Energy 37 (2012) 8395–8401.

[65] L.P. Ma, P. Wang, H.M. Cheng, Improving hydrogen sorption kinetics of MgH_2 by mechanical milling with TiF_3, J. Alloys Compd. 432 (2007) L1–L4.

[66] V.P. Balema, V.K. Pecharsky, K.W. Dennis, Solid state phase transformations in $LiAlH_4$ during high-energy ball-milling, J. Alloys Compd. 313 (2000) 69–74.

[67] V.P. Balema, K.W. Dennis, V.K. Pecharsky, Rapid solid-state transformation of tetrahedral $[AlH_4]^-$ into octahedral $[AlH_6]_3^-$ in lithium aluminohydride, Chem. Commun. 17 (2000) 1665–1666.

[68] C. Duan, Y. Cao, L. Hu, et al., Synergistic effect of TiF_3 on the dehydriding property of α-AlH_3 nano-composite, Mater. Lett. 238 (2019) 254–257.

[69] C.W. Duan, L.X. Hu, D. Xue, Solid state synthesis of nano-sized AlH_3 and its dehydriding behaviour, Green Chem. 17 (2015) 3466–3474.

[70] C.W. Duan, L.X. Hu, J.L. Ma, Ionic liquids as an efficient medium for the mechanochemical synthesis of α-AlH_3 nano-composites, J. Mater. Chem. A 6 (2018) 6309–6318.

[71] C.W. Duan, L.X. Hu, Y. Sun, Reaction kinetics for the solid state synthesis of the $AlH_3/MgCl_2$ nano-composite by mechanical milling, Phys. Chem. Chem. Phys. 17 (2015) 22152–22159.

[72] C.W. Duan, L.X. Hu, Y. Sun, An insight into the process and mechanism of a mechanically activated reaction for synthesizing AlH_3 nano-composites, Dalton Trans. 44 (2015) 16251–16255.

[73] H. Li, F. Guo, M. Kou, A. Famulari, Q. Fu, Gas–solid chemisorption/adsorption and mechanochemical selectivity in dynamic nonporous hybrid metal organic materials, J. Marti-Rujas, Inorg. Chem. 56 (2017) 6584–6590.

[74] M.S. El-Eskandarany, H.S. AlMatrouk, E. Shaban, Hydrogenation/dehydrogenation kinetics study of reacted ball milled $(MgH_2)_{100-x}/(Ni)_y/(Nb_2O_5)_z)_x$ nanocomposite powders, Mater. Today: Proc. 3 (2016) 2735–2743.

[75] L. Jia, K. Kondoh, H. Imai, Nano-scale AlN powders and AlN/Al composites by full and partial direct nitridation of aluminum in solid-state, J. Alloys Compd. 629 (2015) 184–187.

[76] T. Ichikawa, K. Tokoyoda, H. Leng, Hydrogen absorption properties of Li-Mg-N-H system, J. Alloys Compd. 400 (2005) 245–248.

[77] A. Grubisic, X. Li, S.T. Stokes, J. Cordes, G.F. Ganteför, K.H. Bowen, B. Kiran, P. Jena, R. Burgert, H. Schnöckel, Closo-alanes: a new chapter in aluminum hydride chemistry, J. Am. Chem. Soc. 129 (2007) 5969–5975.

[78] S.J. Hwang, R.C. Bowman, J. Graetz, J.J. Reilly, W. Langley, C.M. Jensen, NMR studies of the aluminum hydride phases and their stabilities, J. Alloys Compd. 446 (2007) 290–295.

[79] T.D. Humphries, K.T. Munroe, T.M. DeWinter, C.M. Jensen, G. Sean McGrady, NMR spectroscopic and thermodynamic studies of the etherate and the α, α′, and γ phases of AlH_3, Int. J. Hydrogen Energy 38 (2013) 4577–4586.

[80] D.A. Sheppard, M. Paskevicius, C.E. Buckley, The mechanochemical synthesis of magnesium hydride nanoparticles, J. Alloys Compd. 492 (2010) L72–L74.

[81] E.C. Ashby, J. Prather, The composition of “mixed hydride” reagents. a study of the Schlesinger reaction, J. Am. Chem. Soc. 88 (1966) 729–733.

[82] E. Wiberg, K. Mödritzer, R.U. Lacal, Sobre los halogenalanos y sus compuestos de adición con trimetilamina, Rev. Acad. Cienc. Exactas, Fis. Quim. Nat. Zaragoza 9 (1954) 91.

[83] R. Chen, C.L. Duan, X. Liu, Surface passivation of aluminum hydride particles via atomic layer deposition, J. Vac. Sci. Technol. A 35 (2017) 03E111.

[84] J. Graetz, J.J. Reilly, J.G. Kulleck, Kinetics and thermodynamics of the aluminum hydride polymorphs, J. Alloy. Compd. 446 (2007) 271–275.

[85] R. Shahi, A. Bhatnagar, S.K. Pandey, et al., Effects of Ti-based catalysts and synergistic effect of SWCNTs-TiF_3 on hydrogen uptake and release from MgH_2, Int. J. Hydrogen Energy 39 (2014) 14255–14261.

[86] J.E. Fonneløp, M. Corno, H. Grove, et al., Experimental and computational investigations on the AlH_3/AlF_3 system, J. Alloy. Compd. 509 (2011) 10–14.

[87] G. Sandrock, J. Reilly, J. Graetz, et al., Alkali metal hydride doping of α-AlH_3 for enhanced H_2 desorption kinetics, J. Alloy. Compd. 421 (2006) 185–189.

[88] P. Zhou, J. Zhang, Y. Zhang, et al., Degradation of 2, 4-dichlorophenol by activating persulfate and peroxomonosulfate using micron or nanoscale zero-valent copper, J. Hazard. Mater. 344 (2018) 1209–1219.

[89] P. Jean-Fabien, G. Moussa, U.B. Demirci, et al., Hydrazine borane-induced destabilization of ammonia borane, and vice versa, J. Hazard. Mater. 278 (2014) 158–162.

[90] H. Liu, X. Wang, Z. Dong, G. Cao, Y. Liu, L. Chen, M. Yan, Dehydriding properties of γ-AlH_3, Int. J. Hydrogen Energy 38 (2013) 10851.

[91] I. Gabis, M. Dobrotvorskiy, E. Evard, A. Voyt, Kinetics of dehydrogenation of MgH_2 and AlH_3, J. Alloy. Compd. 509 (2011) S671–S674.

[92] Y. Nakagawa, C.H. Lee, K. Matsui, K. Kousaka, S. Isobe, N. Hashimoto, Y. Kojima, Doping effect of Nb species on hydrogen desorption properties of AlH_3, J. Alloy. Compd. 734 (2018) 55–59.